Composites: Part A 153 (2022) 106747

Contents lists available at ScienceDirect

Composites Part A

journal homepage: www.elsevier.com/locate/compositesa

Effect of secondary particles on the microstructure and mechanical properties of magnetorheological plastomers

Haoming Pang [a,b,1], Yinduan Gao [a,1], Shouhu Xuan [a,*], Xinglong Gong [a,*]

[a] CAS Key Laboratory of Mechanical Behavior and Design of Materials, Department of Modern Mechanics, University of Science and Technology of China (USTC), Hefei 230027, China
[b] College of Mechanical and Electrical Engineering, Qingdao University, 266071, China

ARTICLE INFO

Keywords:
Magnetorheological
Mechanical properties
Microstructure
Particle-reinforcement

ABSTRACT

Magnetorheological plastomers (MRPs) with two different types of fillers have attracted considerable attention for various advantages. However, the effect of secondary particles on mechanical properties is still under controversy due to its conflicting behaviors. In this work, MRPs with three kinds of secondary particles were prepared and their mechanical properties were systemically investigated. The experimental results showed the incorporation of glass balls (20 μm in diameter) led to an increase in the mechanical properties. By contrast, SiO_2 and Fe_3O_4 particles (1 μm in diameter) showed a conflicting behavior. With the increase of secondary particle content, for MRP with SiO_2, the storage modulus first increased and then decreased. But for MRP with Fe_3O_4, the storage modulus first decreased slightly and then increased. At last, the microstructures in MRPs were simulated by a particle-level dynamic method to investigate the effect of secondary particles on the microstructure and mechanical properties of MRPs.

1. Introduction

Magnetorheological plastomer (MRP) is an intelligent magneto-sensitive composite, which is usually composed of magnetically soft particles and a soft polymer [1]. Different from other magneto-rheological (MR) materials, the polymer matrix of MRP is low polymeric. So the MRP can be easily molded into various shapes and behaves like a solid-like MR gel [2,3]. This deformable property of MRP makes it have great potential in flexible sensors [4,5], intelligent drive [6,7] and bionic robots [8,9].

With the development of intelligent driving and sensing, single functional materials can hardly meet the complex application requirements, thus the material design is becoming more and more multifunctional. The matrix of MRP is soft and has good compatibility, therefore, a secondary particle can be added to MRP to realize multi-function. MRPs with two different types of fillers have attracted considerable attention for various advantages, such as structural reinforcements [10], enhanced conductivity [11,12], microwave absorption [13,14], noise absorption [15,16], etc. However, the addition of secondary fillers will affect the evolution of microstructures in MRP, thus affecting the mechanical properties, which may even affect the use of materials. For example, adding too much carbon black will increase the initial modulus of the material and reduce its rheological properties [17].

Until now, some works have studied the effect of secondary particles on the properties of MR materials. According to the magnetic properties, the secondary particles can be divided into magnetic particles and non-magnetic particles. Non magnetic particles usually include carbon black [18], silicon dioxide [19], titanium dioxide [20], etc. The primal aim of adding nonmagnetic particles in the composites is to adjust the initial modulus, decrease the resistance and reduce costs. For example, in 3D printing, the yield stress can be adjusted by changing the content of non-magnetic particles [21]. As for MR materials, in addition to the initial properties, the addition of non-magnetic particles can also affect the magnetorheological effect and the influence is unexpected [22]. Ulicny et al. found an enhancement in the yield stress of MR fluids caused by the presence of non-magnetizable particles and used a three dimensions particle-level simulation to explain the results [23]. Mitsumata et al found that the magneto-elastic behavior of MR elastomer was enhanced by embedding nonmagnetic particles and they concluded that the enhancement was due to the increment of contact between nonmagnetic particles and the particle chain of magnetic particles [24,25].

* Corresponding authors.
E-mail addresses: xuansh@ustc.edu.cn (S. Xuan), gongxl@ustc.edu.cn (X. Gong).
[1] These authors contributed equally

https://doi.org/10.1016/j.compositesa.2021.106747
Received 29 June 2021; Received in revised form 21 November 2021; Accepted 25 November 2021
Available online 27 November 2021
1359-835X/

Rodríguez-Arco et al. also studied the MR properties of a ferrofluid mixed with a diamagnetic microparticle. The results demonstrated the rheological properties were enhanced by dispersing the diamagnetic microparticles [26]. They found the non-magnetic particles could also enhance the magnetic-induced properties of MR materials. But the pre-existing magnetic dipole theory [27–29] could not explain the strengthening effect of non-magnetic particles and they explained the results by simulations. At the same time, the non-magnetic particles also had a negative influence on the mechanical properties. Peng et al. simulated this phenomenon and showed a decrease in the chain length with the addition of non-magnetic particles [30]. For different non-magnetic particles, the effect on the MR properties is different. As for magnetic secondary particles, nickel powder and Fe_3O_4 are commonly used. Liu et al. simulated the microstructure in MR colloidal with superparamagnetic particles. A net-like structure formed and the stress was enhanced [31]. Li et al also found that the adding of Fe_3O_4/NCL could improve the settlement resistance of MRF, but reduce the MR effect [32]. Based on the above research results, it can be found that secondary particles with different magnetic properties have different effects on the microstructure and mechanical properties of MRP. At the same time, even for the same material, the effect of secondary particles with different particle sizes on the macro rheological properties of MRP may be completely opposite. Although several attempts have been made in the theoretical modeling of secondary-filler composites, the knowledge about how the mechanical properties depend on the dimension of secondary fillers is not fully understood. So it is necessary to systematically study the effects of different types of secondary particles on the microstructure and mechanical properties of MRPs

In this paper, three groups of MRP samples with different secondary inclusions were prepared and their mechanical properties were tested. The effects of magnetic properties and particle size of inclusions on the mechanical properties of MRP were studied. Then, the particle-level dynamics method was used to simulate the particle distribution in MRP with different secondary particles, to directly observe the change of particle structure in MRP after inclusion. Combined with the evolution of magnetic potential energy between carbonyl iron powders (CIPs), the influence of the secondary particles on the internal particle structure and macro mechanical properties of MRP was investigated. Finally, the influence of three kinds of secondary particles on the magnetorheological properties of MRP was summarized, which was helpful to the design of MRP materials.

2. Experimental

The raw materials of MRP included polypropylene glycol (PPG-1000, Sinopharm Chemical Reagent Co. Ltd., China), tolylene diisocyanate (TDI, technical grade, 80%, Sigma-Aldrich, USA), and diethylene glycol (DEG, Sinopharm Chemical Reagent Co. Ltd., Shanghai, China),

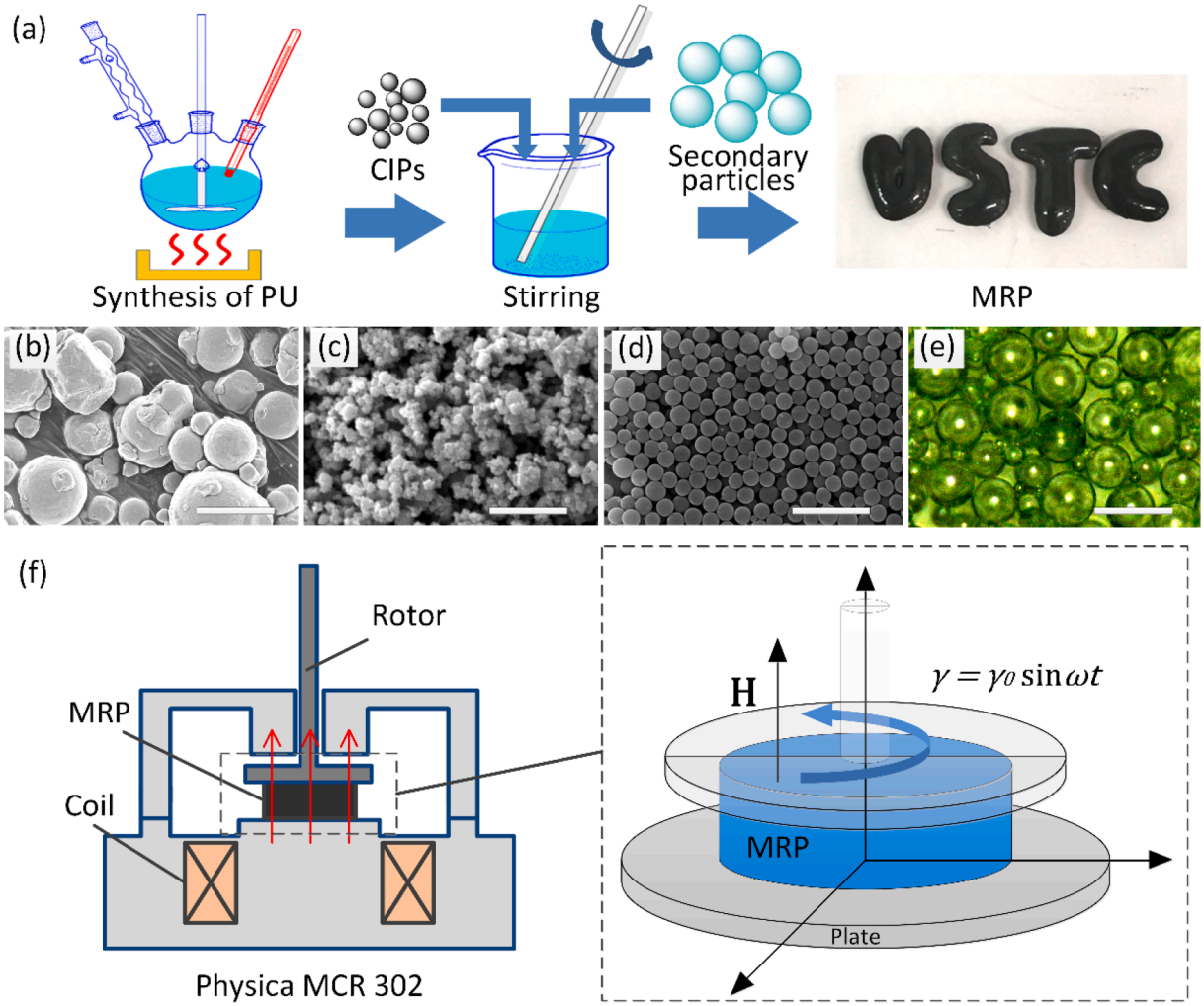

Fig. 1. Schematic illustration of the preparation and test of MRPs. (a) Schematic diagram of the fabrication process and the optical image of MRP. Scanning electron microscope (SEM) images of (b) CIPs, (c) Fe_3O_4 particles, and (d) SiO_2 particles. The scale bars in (b-d) are 5 μm. (e) Optical image of HGPs. Scale bar is 30 μm. (f) Schematic diagram of the rheometer and the configuration of the MRP.

carbonyl iron powder (CIP, type CN, 6 μm average diameter, BASF aktiengesellschaft, Germany), non-magnetic hollow glass powder (HGP, type C70, 20 μm average diameter, zhongkehuaxing new materials Co. Ltd, China), non-magnetic SiO_2 powder (B117, 1 μm average diameter, Bowei Applied Materials Technology Co. Ltd, China), and Fe_3O_4 powder (CAS:1317–61–9, 1 μm average diameter, Bowei Applied Materials Technology Co. Ltd, China).

In this paper, three grouds of MRP with different secondary particles were prepared and the secondary particles were HGP, SiO_2, and Fe_3O_4, respectively. CIPs and secondary fillers were dispersed in a homemade polyurethane (PU) to prepare MRPs (Fig. 1**a**). Firstly, TDI and PPG were added to the flask with a molar ratio of 3:1 at 80 ℃ for 2 h. Then, the reaction temperature was reduced to 40 ℃, and DEG was added to the reactor. Raised the temperature to 60 ℃ and hold for about 30 min. Thus homemade PU matrix was synthesized. At last, different amounts of CIPs and secondary particles were added into PU immediately by vigorously stirring until they were mixed well. The content of different particles is shown in Table 1. All filler contents in the text refer to volume fraction and are represented by φ.

In this paper, three kinds of secondary particles were selected: Fe_3O_4 particles (Fig. 1**c**), SiO_2 particles (Fig. 1**d**), and HGPs (Fig. 1**e**). The most commonly used magnetic particles in MRP are CIPs (Fig. 1**b**), so we take CIPs as the main particles. In addition to CIPs, the most commonly used magnetic particles are Fe_3O_4, so Fe_3O_4 was selected as the magnetic secondary particles. Spherical Fe_3O_4 is usually prepared by chemical synthesis and its diameter is smaller than that of CIPs. Here the average diameter of Fe_3O_4 is about 1 μm. For non-magnetic particles, two kinds of particles with different particle sizes were selected. As shown in Fig. 1, the diameter of SiO_2 is about 1 μm (the same as that of Fe_3O_4), and HGP is 20 μm in diameter (much larger than that of CIPs). The three kinds of particles were selected to study the effects of particle sizes and magnetic properties on the microstructure and macroscopic properties of MRP.

The MR properties of all the MRPs were tested on a commercial rheometer (Physica MCR302, Anton Paar Co., Austria) equipped with a magneto-controllable accessory MRD180 and temperature control module (Fig. 1**f**). Before the test, the MRP was placed between the rotor and the plate, with a diameter of 20 mm and a thickness of 1 mm. Two magnetic skeletons are placed outside the sample to create a magnetic field perpendicular to the bottom of the MRP, the strength of the magnetic field can be regulated by an electric current. The storage modulus of MRP was measured in the sinusoidal oscillation shear mode. During the testing, sinusoidal oscillation of the rotor exerted shear on the sample, and the shear strain and torque were tested at the same time. Then the storage modulus of the MRP was obtained by processing the signal. The test frequency was 5 Hz and the strain amplitude was 0.1%. The morphologies of the MRPs were imaged by a scanning electron microscope (Gemini 500, Carl Zeiss Jena, Germany). The Chamber SE Detector was used and the accelerating voltage was set as 20 kV. The magnetization curves of MRP were tested by a HyMDC (Hysteresis Measurement of Soft and Hard Magnetic Materials, Metis Instruments & Equipment NV Co., Belgium).

Table 1
Compositions of MRP samples.

Sample no.	Group 1				
CIP (vol%)	9	9	9	9	9
HGP (vol%)	0	4.5	9	13.5	18
Sample no.	Group 2				
CIP (vol%)	9	9	9	9	9
SiO_2 (vol%)	0	4.5	9	13.5	18
Sample no.	Group 3				
CIP (vol%)	9	9	9	9	9
Fe_3O_4 (vol%)	0	4.5	9	13.5	18

3. Results and discussion

3.1. Effect of non-magnetic inclusions on the microstructure of MRPs

Firstly, the effect of non-magnetic inclusions (HGPs and SiO_2 particles) on the microstructure and MR properties of MRPs is studied. The morphologies of MRP with different non-magnetic inclusions are shown in Fig. 2**a and b**. It can be seen from the scanning electron microscope (SEM) images that under the action of a magnetic field, the CIPs are connected head to tail to form a chain-like structure (inside the yellow curve in Fig. 2**b**) along the direction of the magnetic field. Non-magnetic HGP and SiO_2 are dispersed uniformly in the PU matrix. Since non-magnetic particles are not affected by the magnetic dipole force in the magnetic field (**Fig. S1**), their positions are only related to the movement of CIPs. However, because the particles are well wrapped by the PU, it is difficult for the electron beam to penetrate through the PU layer and observe the detailed structures between particles. So, SEM images show little difference in the CIP structures of MRPs with different non-magnetic particles and it is difficult to further study the effect of non-magnetic particles on the internal structure of MRP.

For MRP, small changes in CIP structure will have a great impact on the mechanical properties of materials. As shown in Fig. 2**c and d**, the storage modulus and their variation tendencies of MRP with different non-magnetic particles are different. For MRPs with HGPs, both the initial storage modulus (storage modulus without applying a magnetic field) and saturated storage modulus (maximum storage modulus under the magnetic field) increase with the increasing HGP content, the MR properties of the material are greatly enhanced. For MRPs with different contents of SiO_2 particles, the initial storage modulus increases slightly with the increasing SiO_2 content, but the saturated storage modulus reaches the maximum when the SiO_2 content is 9%, and then decreases with the further increase of SiO_2 content. For the same inclusion content, when the size of non-magnetic particles is different, the effect on the storage modulus of MRP is opposite. These results indicate that non-magnetic particles with different sizes have different effects on the microstructure of MRP.

To further explore the effect of non-magnetic particles with different particle sizes on the mechanical properties of MRP, the internal microstructure of MRP is simulated by a particle-level dynamics method. In the calculation process, firstly, the particle position is randomly generated. Then the force on each particle is analyzed and the motion equation is established. Finally, the equation of motion is solved repeatedly until the system reaches stability. At this time, the position coordinates of each particle are obtained. In the calculation process, the force between the particles and the force between the particles and the matrix are considered. When a magnetic particle with a diameter d_i is placed into a uniform magnetic field $\boldsymbol{H}$, the magnetic moment $\boldsymbol{m}_i$ of the particle is:

$$\boldsymbol{m}_i = \boldsymbol{m}_s\left(1 - e^{-\chi H}\right)V \tag{1}$$

where $\boldsymbol{m}_s$ is the saturated magnetization of the magnetic particle, $V = \pi d_i^3/6$ is the volume of particle i, and χ is the adaptive magnetization coefficient. Here, $\chi = 5.06 \times 10^{-6}\mathrm{m/A}$, $\boldsymbol{m}_s = 1.38 \times 10^6\mathrm{A/m}$ for CIPs, $\boldsymbol{m}_s = 4.18 \times 10^5\mathrm{A/m}$ for Fe_3O_4 particles, and $\boldsymbol{m}_s = 0$ for HGPs and SiO_2 particles.

The dipole force between two particles is given by:

$$\boldsymbol{F}_{ij}^{dipole} = -\frac{3\mu_0}{4\pi r_{ij}^4}c_m\left[\boldsymbol{m}_i\bullet\boldsymbol{m}_j\hat{\boldsymbol{r}} + \boldsymbol{m}_i\bullet\hat{\boldsymbol{r}}\boldsymbol{m}_j + \boldsymbol{m}_j\bullet\hat{\boldsymbol{r}}\boldsymbol{m}_i - 5(\boldsymbol{m}_i\bullet\hat{\boldsymbol{r}})(\boldsymbol{m}_j\bullet\hat{\boldsymbol{r}})\hat{\boldsymbol{r}}\right] \tag{2}$$

Where r_{ij} represents the distance between two particles, μ_0 is the magnetic permeability of the matrix. c_m is the correction factor of the point dipole model [33]. $\boldsymbol{r}$ is the position vector from particle i to particle j and $r = |\boldsymbol{r}|$, $\hat{\boldsymbol{r}} = \boldsymbol{r}/r$.

To prevent particles from overlapping, a repulsive force $\boldsymbol{F}_{ij}^{ev}$ is also introduced:

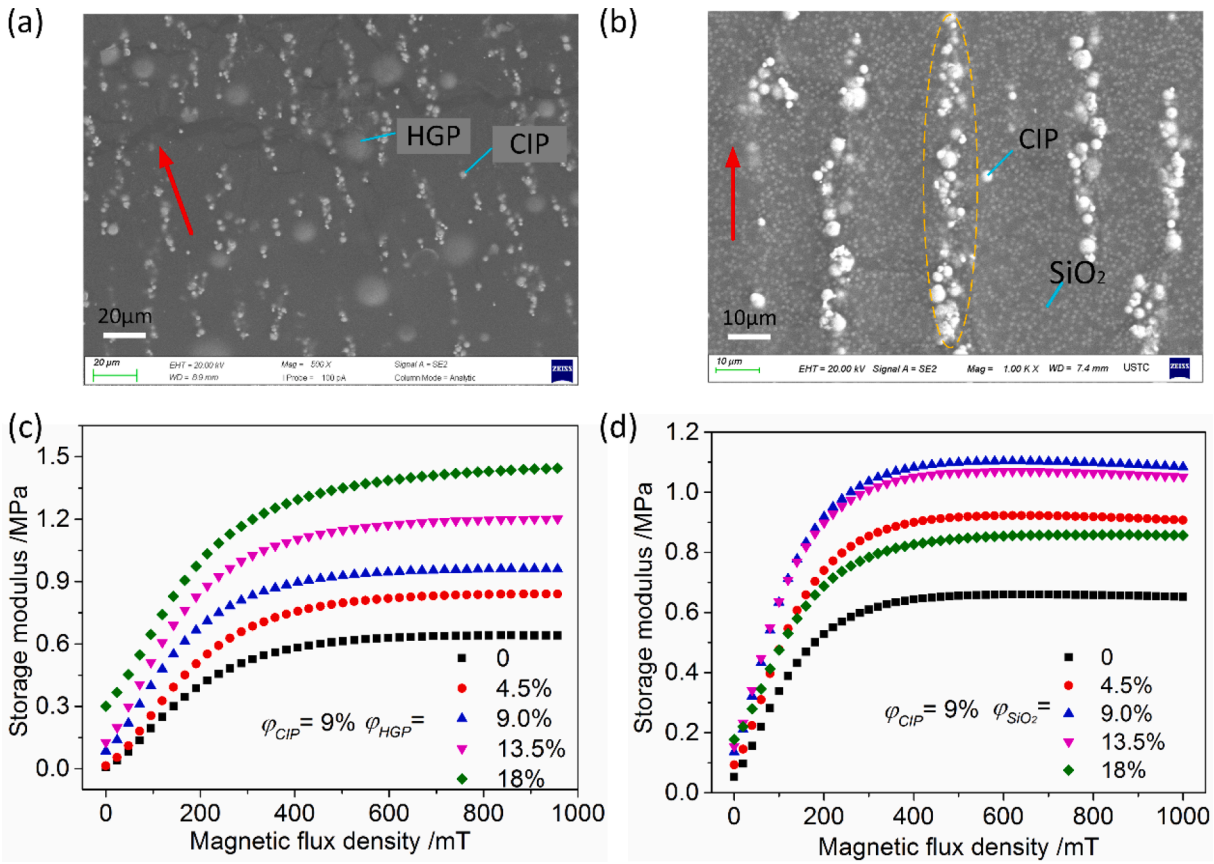

Fig. 2. The micromorphology and mechanical properties of MRP with different non-magnetic particle inclusions. (a) SEM image MRP with 18% HGPs. (b) SEM image of MRP with 18% SiO_2 particles. The red arrows indicate the direction of the magnetic field. The shear storage modulus changes of MRP with different contents of (c) HGPs and (d) SiO_2 particles. φ stands for volume fraction.

$$\boldsymbol{F}_{ij}^{ev} = -\frac{3\mu_0 m_{si} m_{sj}}{2\pi d_{ij}^4}\frac{2V_i}{V_i+V_j}10^{-10\left(\frac{r_{ij}}{d_{ij}}-1\right)}\hat{\boldsymbol{r}} \tag{3}$$

Here, m_{si} and m_{sj} are the saturation magnetization of the target particles. As for HGPs and SiO_2 particles, the magnetization $m_{si} = 1.38\times10^6 V_i$, when calculating the repulsive force.

The inter-particle van der Waals force can be expressed as [34]:

$$\boldsymbol{F}_{ij}^{vdw} = \frac{A}{24}\frac{d_{ij}}{L_r^2}\hat{\boldsymbol{r}} \tag{4}$$

where $A = 5\times10^{-19}$ J is the Hamaker constant and $L_r = \max[r_{ij}-d_{ij}, 0.001d_{ij}]$. The resultant gravity and buoyancy forces acting on a particle can be expressed as:

$$\boldsymbol{F}_i^g = \frac{\pi d_i}{6}(\rho-\rho_m)\boldsymbol{g} \tag{5}$$

where ρ and ρ_m are the densities of the particle and the matrix, respectively, and $\boldsymbol{g}$ is the gravitational acceleration. In both simulations and experiments, the motion of particles related to the Bingham fluid has an extremely low Reynolds number. Hence, the hydrodynamic drag force is:

$$\boldsymbol{F}_i^d = -\frac{19}{8}\pi\left(\tau_0 d_i^2\hat{\boldsymbol{v}} + d_i\eta\boldsymbol{v}\right) \tag{6}$$

where τ_0 is the shear yield stress of the matrix, η is the viscosity of the matrix, and $\hat{\boldsymbol{v}}$ is the unit vector of velocity relative to the surrounding matrix. Because of the yield stress in the matrix, when $|\sum F_i| \le \frac{19}{8}\pi\tau_0 d_i^2$, particles will not move. Where $\sum F_i$ denotes the total force, excluding the hydrodynamic drag force on particle i. Regardless of the inertia and acceleration of the particle, the equation of motion is established as follows:

$$\sum_{j\neq i}\left(\boldsymbol{F}_{ij}^{dipole} + \boldsymbol{F}_{ij}^{vdW} + \boldsymbol{F}_{ij}^{ev}\right) + \boldsymbol{F}_i^d + \boldsymbol{F}_i^g = 0 \tag{7}$$

Eq. (7) can be solved using a numerical method to get the particle microstructure. As shown in Fig. 3, the simulated particle microstructure in MRP doped with HGPs is similar to that of the SEM image. The adding of HGP particles does not hinder the formation of the chain-like structure of CIPs, but distributes between CIP chains, forming a three-dimensional structure together with CIPs. Therefore, with the increase of HGP content, the storage modulus of the MRP increases. For the MRP with SiO_2 particles, the simulated results show more details. It can be found that when the content of SiO_2 is 9%, most SiO_2 particles are evenly distributed in the matrix. In this case, SiO_2 particles have the same effect as HGP particles. As a reinforcing term of particle reinforced composite, the storage modulus of the materials is improved by the non-magnetic particles. Obviously, we can also find that some SiO_2 particles on the moving path of CIPs are pushed by CIPs and gather around the CIPs to form chain-like structures. These SiO_2 particles can strengthen the particle chains, Therefore, when the content of non-magnetic particles is less than 9%, with the same particle content, the storage modulus of the MRP with SiO_2 particles is higher than that of MRP with HGPs.

However, with the further increase of SiO_2 particles, SiO_2 particles around the CIPs will hinder the further evolution of the CIP chains. On the one hand, when the CIP chains are close to each other to form a columnar structure, the SiO_2 particles around the CIPs will hinder the magnetic particles from approaching each other and increase the distance between the CIPs (left image in Fig. 3**e**). On the other hand, too many SiO_2 particles will increase the resistance of CIPs when they move,

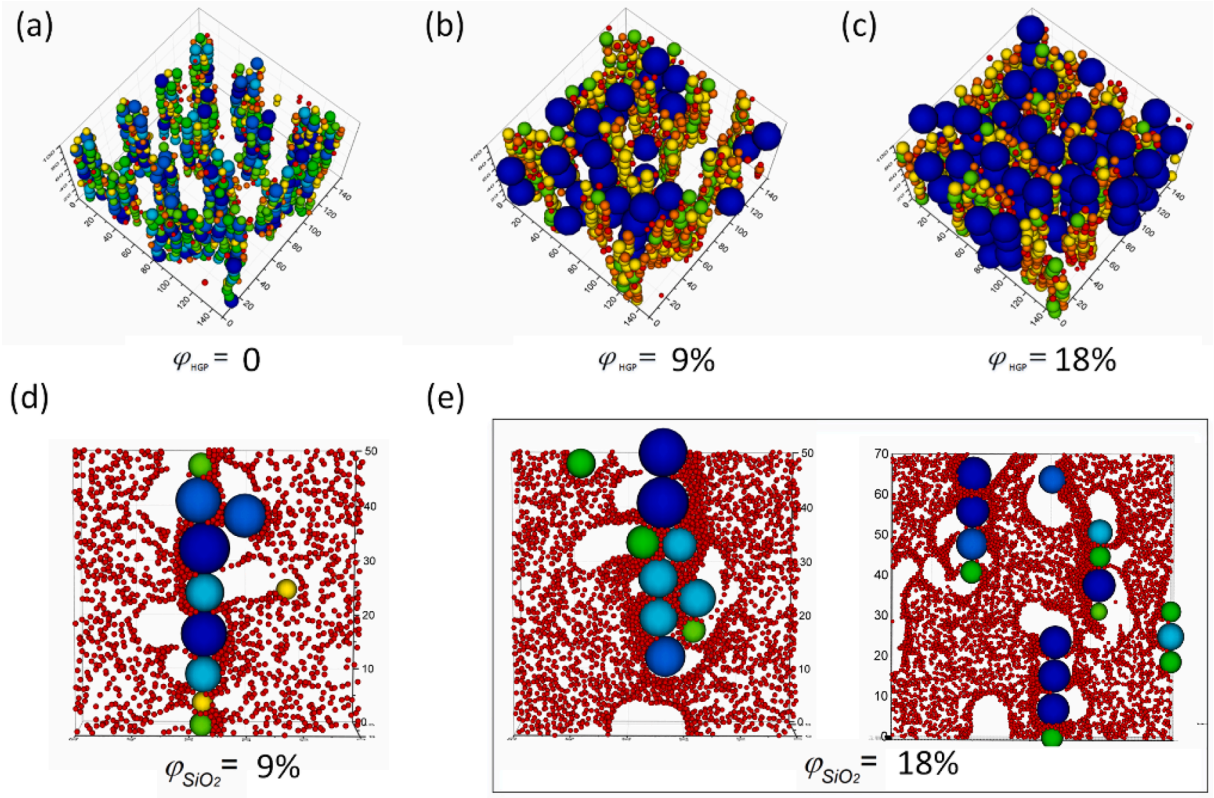

Fig. 3. Simulated results of microstructure in MRP with different non-magnetic particles. The internal microstructure of MRP with different HGP contents. Large blue balls represent HGPs. (a) $\varphi_{HGP} = 0$, (b) $\varphi_{HGP} = 9$, (c) $\varphi_{HGP} = 18$. The internal microstructure of MRP with different SiO_2 contents. (d) $\varphi_{SiO2} = 9\%$, (e) $\varphi_{SiO2} = 18\%$. Fig. 2d and e only show the microstructure in the area with a thickness of 7 μm for easy observation. Small red balls represent SiO_2 particles.

which makes it difficult for CIPs to form a long-chain structure, but a short cluster structure composed of four or five CIPs (right image in Fig. 3**e**). At this time, the adding of too many SiO_2 particles will increase the average distance between CIPs, reduce the interaction between the magnetic particles, and result in the decrease of the saturated storage modulus of the MRP.

To further explore the effect of SiO_2 particles on the microstructure of MRP, the three-dimensional structures of SiO_2 particles doped MRP in the magnetic field are simulated and the magnetic potential energy between particles $U_m(\text{inter}-\text{particle})$ is shown in Fig. 4. Here $U_m(\text{inter}-\text{particle})$ is proposed as:

$$U_m(\text{inter}-\text{particle}) = \mu_0 \sum_i \sum_{j>i} \frac{1}{4\pi r_{ij}^3} \left(\boldsymbol{m}_i \cdot \boldsymbol{m}_j - 3\boldsymbol{m}_i \cdot \hat{\boldsymbol{r}} \boldsymbol{m}_j \cdot \hat{\boldsymbol{r}}\right) \quad (8)$$

$U_m(\text{inter}-\text{particle})$ depends on the particle's position, interaction, and distribution in the matrix, which can reflect the evolution of the microstructure. It can be seen that when the content of SiO_2 particles is 13.5%, the existence of SiO_2 particles will hinder the movement of CIPs. In Fig. 3b, there are SiO_2 particles between two adjacent CIPs and there

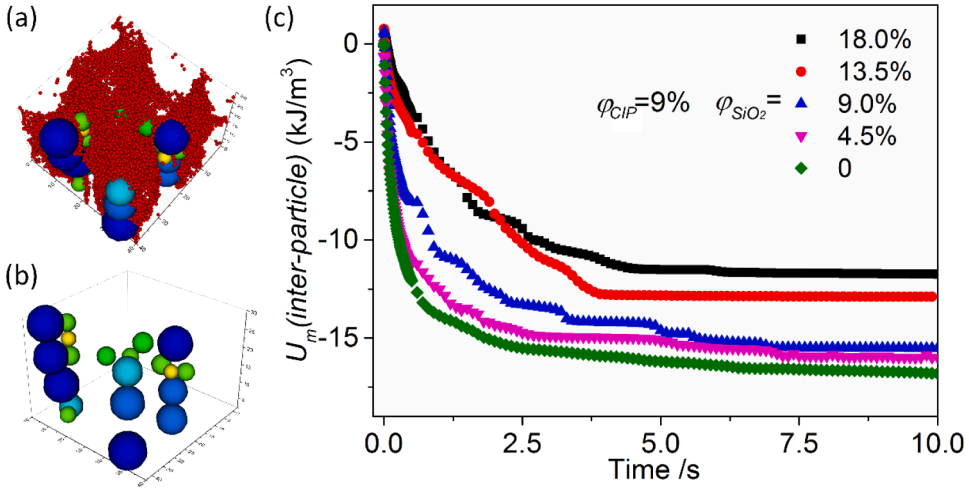

Fig. 4. (a) The three-dimensional structure of MRP with 13.5% SiO_2 particles under magnetic field. (b) The three-dimensional CIP structure of MRP with 13.5% SiO_2 particles. Fig. 2b only shows the CIPs in Fig. 2a for convenience observation. (c) The calculated magnetic potential energy U_m(inter-particle) changes with time in MRP with different SiO_2 contents.

are some SiO_2 particles between the columnar structure formed by CIPs, which makes the structure of CIPs sparse. The calculated magnetic potential energy U_m(inter-particle) between particles shows that the reduction of U_m(inter-particle) between particles decreases with the increasing SiO_2 particle content. Under the action of the magnetic field, the magnetic particles will move and recombine, making the magnetic potential energy of the whole system reach the lowest. The more the U_m(inter-particle) between particles decreases, the more stable the structure of magnetic particles is under the action of the magnetic field. Fig. 4**c** shows that with the increasing content of SiO_2 particles, the reduction of U_m(inter-particle) decreases, which indicates that SiO_2 particles hinder the movement of some CIPs. In particular, when the content of SiO_2 particles exceeds 9%, the decrease rate of U_m(inter-particle) is rapidly slowed down, resulting in the decrease of the saturated storage modulus of MRP. It is worth noting that the U_m(inter-particle) is also increased when the content of SiO_2 particles is less than 9%, but the saturated storage modulus of MRP still increases. This is because as a particle reinforcing composite, the modulus of SiO_2 particles is much higher than the bulk modulus of PU. The addition of SiO_2 particles can enhance the overall storage modulus of MRP. Meanwhile, an appropriate amount of SiO_2 particles around the CIP chains can also strengthen the CIP chains and improve the mechanical properties of MRPs.

3.2. *Effect of magnetic Fe_3O_4 inclusion on the microstructure of MRPs*

To study the effect of magnetic secondary particles on the microstructure and mechanical properties of MRPs. Fe_3O_4 particles are selected as the secondary particles because they are commonly used and the size of Fe_3O_4 particles is uniform. The magnetization curves of Fe_3O_4 particles and CIPs are shown in **Fig. S2** and the saturated magnetizations of Fe_3O_4 particles are lower than that of CIPs. MRPs with different Fe_3O_4 particles are prepared and tested, and their micromorphology is observed. Due to the good adhesion of the PU matrix, the magnetic particles in MRP are wrapped by PU. The precision of SEM images is limited by the depth of electron beam can breakdown. It can be roughly distinguished from Fig. 5**a and b** that the larger particles are CIPs, and some CIPs form chain-like structures along the magnetic field. The Fe_3O_4 particles with smaller particle sizes form beaded structures connected end to end due to their uniform particle size and these beads are evenly distributed in the matrix.

Because Fe_3O_4 particles are soft magnetic particles, the addition of Fe_3O_4 particles will affect the magnetic properties of MRP. The magnetization curves of MRPs with different Fe_3O_4 particles are tested and shown in Fig. 5**c**. Here, the unit of magnetization is emu/cm^3 because the content of internal particles is distinguished by volume fraction, which is convenient for comparison. It can be seen that with the increase of Fe_3O_4 content in the MRPs, the saturated magnetization of the MRP increases gradually indicating that the overall magnetism of the sample is enhanced. As for the mechanical properties, it can be seen from Fig. 5**d** that when the content of Fe_3O_4 particles is less than 9%, the storage modulus of MRP has little change. Especially for the MRP with 9% Fe_3O_4 particles, the storage modulus decreases but the saturated magnetization is greater than that of MRPs without Fe_3O_4 particles, which is the opposite of general cognition. With the further increase of Fe_3O_4 content, the storage modulus increases rapidly. The effect of Fe_3O_4 particles on the mechanical properties of MRP is abnormal when the volume fraction of Fe_3O_4 particles is less than 9%, which is necessarily related to the microstructure in the Fe_3O_4 particles doped MRPs.

To explore the mechanism of Fe_3O_4 particles on the mechanical properties of MRPs, the internal structures of MRPs with different Fe_3O_4 contents are simulated by the particle-level dynamics method. Fig. 6**a**

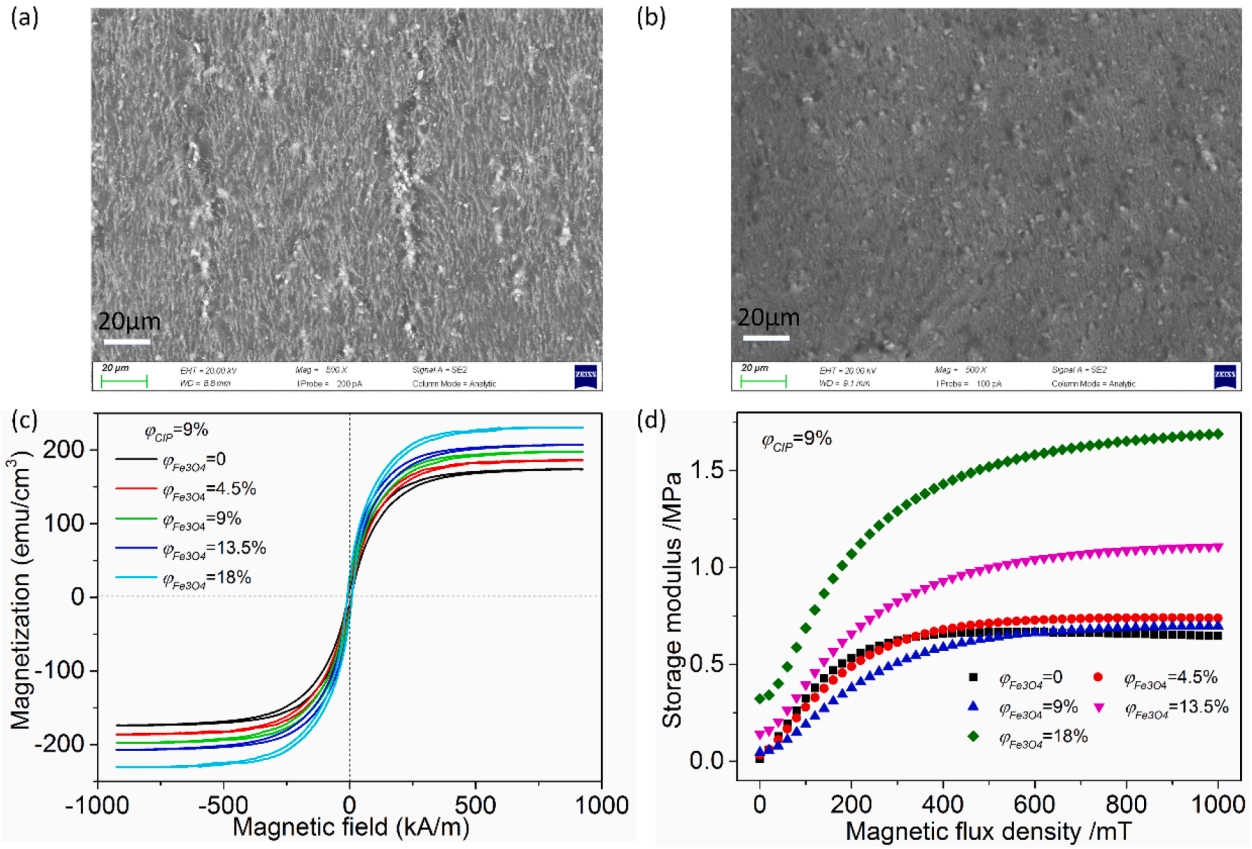

Fig. 5. The micromorphology and mechanical properties of MRP with different Fe_3O_4 particles. (a) SEM image MRP with 9% Fe_3O_4 particles. (b) SEM image MRP with 18% Fe_3O_4 particles. (c) Magnetization curves of MRP with different Fe_3O_4 particles. (d) The shear storage modulus changes of MRP with different contents of Fe_3O_4 particles.

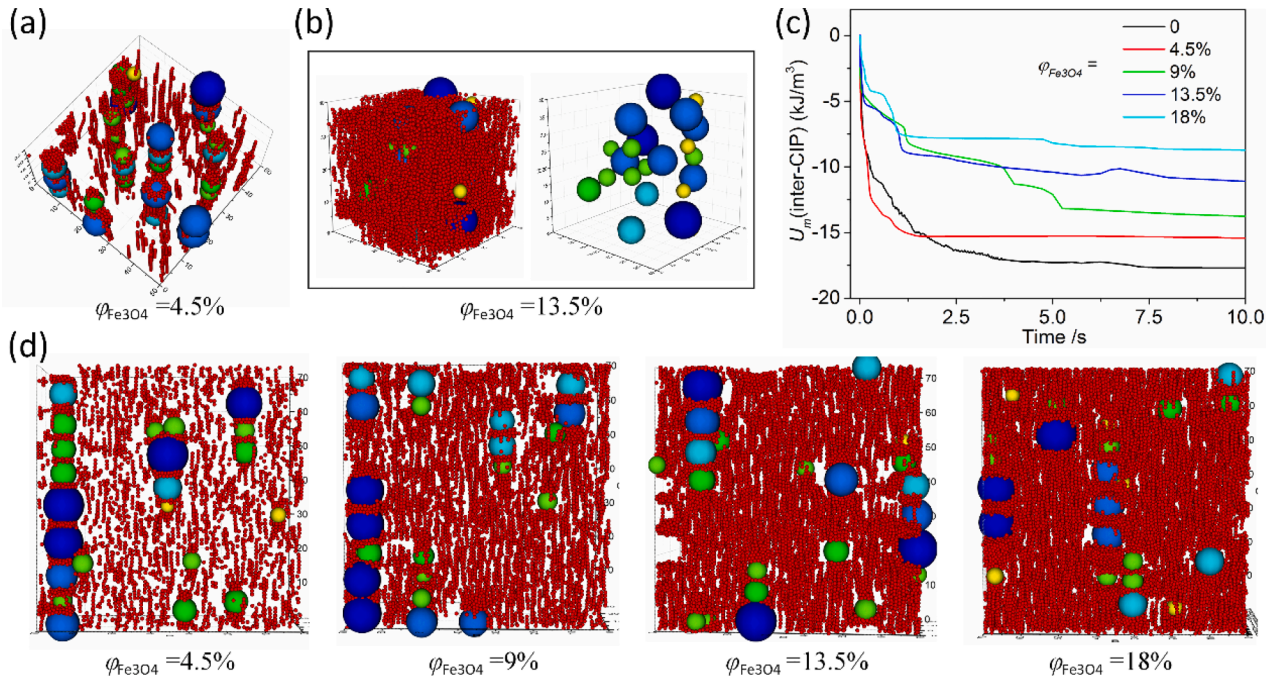

Fig. 6. (a) Three-dimensional microstructure of MRP with 4.5% Fe_3O_4 particles under magnetic field. Small red balls represent SiO_2 particles. (b) Three-dimensional structure of MRP with 13.5% Fe_3O_4 particles. The left image shows all particles in the sample and the right image only shows the CIPs in the MRP for convenience observation. (c) The magnetic potential energy between CIPs U_m(inter-CIP) changes with time in MRP with different Fe_3O_4 contents. (d) The internal microstructure of MRP with different Fe_3O_4 contents. Here, only the microstructures in the area with a thickness of 7 μm are showed for easy observation.

and b show the three-dimensional microstructures of MRPs with different Fe_3O_4 particle contents. It can be seen that these structures are very different from those in Fig. 3**a**. Combined with Fig. 6**d**, it can be found that when the volume fraction of Fe_3O_4 particles is less than 9%, CIPs combined with some Fe_3O_4 particles form a single chain-like structure and there is no trend of merging between the chains. The rest of the Fe_3O_4 particles form beaded structures and distribute among the chains of CIPs. When the volume fraction of Fe_3O_4 particles is greater than 9%, the length of CIP chains is shortened, even some CIPs are distributed in Fe_3O_4 chains alone (Fig. 6**b**). In the MRP without Fe_3O_4 particles (Fig. 3**a**) because the particle size of CIP is lognormal distribution, the particle size range is 3–14 μm. Under the action of the magnetic field, CIPs first form a beaded structure like Fe_3O_4 chains. However, due to the wide range of particle size distribution, the interface diameter of the single-chain is different along the direction of the magnetic field, so the interaction force between the chains is different, resulting in the contact between CIP chains to form a more compact columnar structure (Fig. 3**a**). For MRPs with magnetic Fe_3O_4 particles, after CIPs form beaded structures, Fe_3O_4 chains with smaller particle sizes will preferentially fill between the CIP chains, weaken the attraction between the CIP chains, and then prevent the CIP chains from approaching and merging with each other. With the further increase of Fe_3O_4 particles, Fe_3O_4 between CIPs will also form particle chains under the action of a magnetic field, which prevents the CIPs from getting close to each other, so that some CIP are isolated and distributed in the matrix alone. As can be seen from the magnetic potential energy between CIPs U_m(inter-CIP) in Fig. 6**c**, the final magnetic potential energy increases gradually with increasing Fe_3O_4 content. Here U_m(inter-CIP) represents the magnetic potential energy between CIPs and is calculated by Eq. (8) for all CIPs, excluding Fe_3O_4 powders. The change of U_m(inter-CIP) reflects the evolution of CIPs in MRP. It can be seen from Fig. 6**c** that the shape of the curve of the MRP with 4.5% Fe_3O_4 is basically the same as that without Fe_3O_4 particles, but the time to reach stability becomes shorter and the final magnetic potential energy increases, which indicates that the Fe_3O_4 particles only hinder the merging of CIP chains to form a columnar structure. For MRPs with Fe_3O_4 content greater than 4.5%, the curves first drop to a value and then tends to be stable. That is because Fe_3O_4 particles form chains between CIPs, which hinder the CIPs forming chains. For MRP with 9% Fe_3O_4 particles, some CIPs can overcome the obstruction of Fe_3O_4 particles and move, so the magnetic potential energy will decrease. However, the magnetic potential energy between CIPs increases, and the interaction between CIPs decreases. But on the other hand, Fe_3O_4 is also a kind of magnetic particle, with the increase of Fe_3O_4 particle content, the decrease of magnetic potential energy between all particles U_m(inter-particles) increases (**Fig. S3**), which will lead to the increase of the storage modulus. Therefore, with the increase of Fe_3O_4 content, on the one hand, the increase of the overall magnetic particle content in the material will increase the mechanical properties of the material. On the other hand, the addition of Fe_3O_4 particles will hinder the movement of CIP and prevent CIPs from forming chain-like structures, which will reduce the mechanical properties of the MRP. The two factors together lead to that when the content of Fe_3O_4 is less than 9%, the addition of Fe_3O_4 will not increase the storage modulus of MRP, but further increase the content of Fe_3O_4, the saturated storage modulus of MRP will increase rapidly.

Based on the above test and numerical simulation, we can conclude that both the magnetic properties and particle sizes of the secondary particles have important effects on the microstructure and mechanical properties of MRP. The initial storage modulus G_0, saturated storage modulus G_s, and magnetic-induced storage modulus ΔG' ($\Delta G' = G_s - G_0$) of MRP with different secondary particles are shown in Fig. 7**a–c**. Without a magnetic field, the G_0 of three groups of MRP increases with increasing secondary particle content. The modulus of these particles is higher than that of the PU matrix. The secondary particles work as reinforcing inclusions of the particle reinforced composite and improve the shear modulus of the material. Among them, when the particle content is less than 9%, the reinforcement effect of SiO_2 particles is the most obvious, so it is often used to adjust the initial rheological properties of materials. When the particle content is higher than 9%, the enhancement effect of HGP and Fe_3O_4 is better. As for G_s and ΔG', the reinforcing effect of the three kinds of particles is different with increasing particle content. As for HGPs, because the particle size of HGP

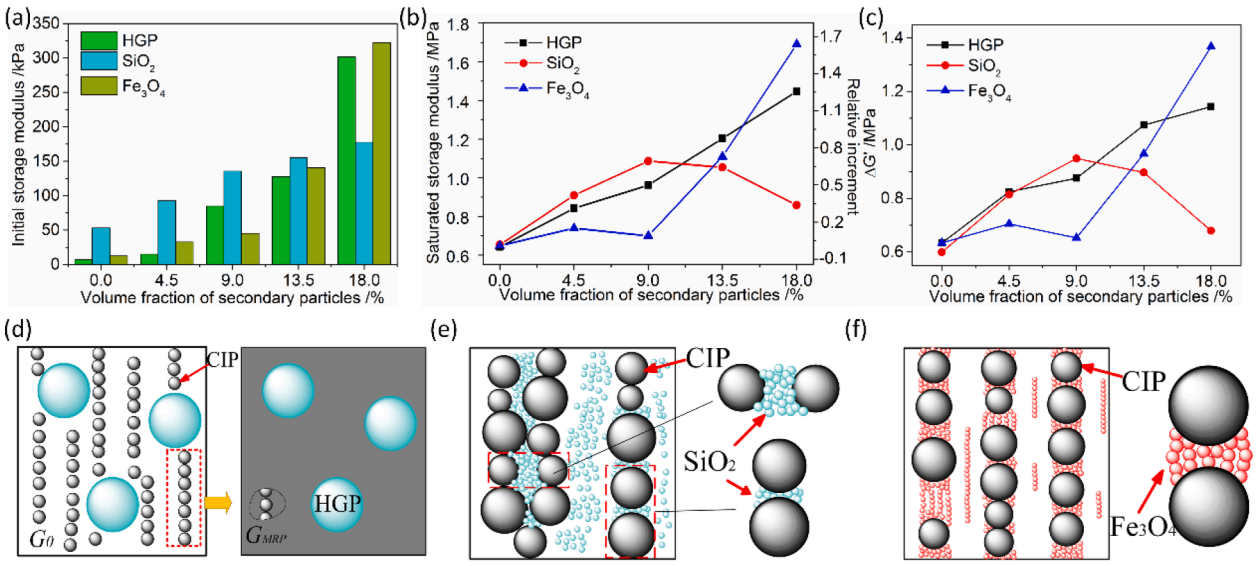

Fig. 7. (a) Initial storage modulus G_0, (b) saturated storage modulus G_s, and (c) magnetic-induced storage modulus ΔG' of MRP with different secondary inclusion particles. Schematic diagram of MRP with different secondary inclusion particles: (d) HGPs, (e) SiO_2, and (f) Fe_3O_4.

is larger than that of CIP, the addition of HGP has little effect on the microstructure of CIPs. Thus, as shown in Fig. 7**d**, under applying a magnetic field, MRP containing two kinds of particles can be equivalent to a particle reinforced composite with HGP adding into the matrix, where the MRP containing PU and CIPs becomes the matrix of the composite and HGPs are added into the new matrix. Then G_s can be expressed according to Mori-Tanaka's method as [35]:

$$G_s(\varphi_{HGP}) = G_s(0) \times \left(1 + \frac{k\varphi_{HGP}}{1-\varphi_{HGP}}\right) \tag{9}$$

Where φ_{HGP} is the volume fraction of HPG, k is the correction factor, and $G_s(0)$ is the saturated storage modulus without HGPs. G_s increases from 0.64 MPa to 1.44 MPa with increasing HGP content, increasing about 125%. ΔG' also increases with the increasing HGP content, and the maximum ΔG' can reach 1.14 MPa (80% increment).

As for SiO_2 particles and Fe_3O_4 particles, taking 9% content as the dividing line, they have opposite effects on G_s and ΔG' of MRP in different regions. For MRP with SiO_2 particles, when the particle content is less than 9%, the SiO_2 particles can strengthen the CIP chains, so G_s increases with the increase of SiO_2 content. The maximum G_s is 1.08 MPa, which is higher than that of MRP with 9% HGP (0.96 MPa). But with the further increase of SiO_2 particles, too many SiO_2 will hinder the movement of CIPs and reduce the storage modulus of MRP (Fig. 7**e**). On the contrary, when the particle content is less than 9%, G_s of MRP with Fe_3O_4 particles basically unchanges. That is because the adding of a small amount of Fe_3O_4 particles will prevent the CIP chains from forming a more stable columnar structure, which counteracts the enhancement effect of the Fe_3O_4 particles themselves (Fig. 7**f**). However, when the particle content is more than 9%, G_s increases rapidly, and the maximum G_s can reach to 1.69 MPa, which is the maximum G_s of the three groups of MRPs. In a word, the three kinds of particles have their own advantages and disadvantages in different content ranges, and various mechanical properties of MRP can be achieved by choosing the type of particles according to their needs.

4. Conclusion

In summary, the influence of the secondary particles on the microstructure and mechanical properties of MRP is studied by experimental research and numerical simulation. Three kinds of particles are selected as secondary particles. They were non-magnetic HGP (20 μm in diameter), non-magnetic SiO_2 particles (1 μm in diameter), and magnetic Fe_3O_4 particles (1 μm in diameter), respectively. The experimental results show that both the magnetic properties and size of the secondary particles have important effects on the mechanical properties of MRP. Among them, HGP can enhance the mechanical properties of MRP all the time. When the particle content is less than 9%, the reinforcement effect of SiO_2 is the best. When the content of MRP is 18%, the storage modulus of MRP with Fe_3O_4 is the largest. To understand the influence mechanism of particles on the mechanical properties of MRP, the microstructure of MRP with the different secondary particles is simulated by a particle-level dynamics method. The results show that HGP particles have little effect on the arrangement of CIPs, so the storage modulus of MRP increases with the increase of HGP content. For SiO_2 particles, when the content is less than 9%, it can strengthen the chain of CIPs. But when the content is more than 9%, it will hinder the movement of CIPs and reduce the storage modulus. For Fe_3O_4 particles, when the content is less than 9%, it will prevent the CIP chains from approaching each other, so the storage modulus of MRP basically unchanges. Based on the above analysis, by adding different magnetic and particle size particles, the internal microstructure and the mechanical properties of MRP can be adjusted to meet different application needs.

CRediT authorship contribution statement

Haoming Pang: Conceptualization, Investigation, Methodology, Software, Writing – original draft. **Yinduan Gao:** Formal analysis, Data curation. **Shouhu Xuan:** Project administration, Validation, Funding acquisition, Writing – review & editing. **Xinglong Gong:** Supervision, Resources, Funding acquisition, Writing – review & editing.

Declaration of Competing Interest

The authors declare that they have no known competing financial interests or personal relationships that could have appeared to influence the work reported in this paper.

Acknowledgments

This work was supported by the National Natural Science Foundation of China (Grant Nos. 12102424, 12132016, 11972343, 11822209), the Anhui's Key R&D Program of China (Grant No. 202104a05020009), and the Strategic Priority Research Program of the Chinese Academy of Sciences (Grant No. XDB22040502).

Appendix A. Supplementary material

Supplementary data to this article can be found online at https://doi.org/10.1016/j.compositesa.2021.106747.

References

[1] Xu YG, Gong XL, Xuan SH, Zhang W, Fan YC. A high-performance magnetorheological material: preparation, characterization and magnetic-mechanic coupling properties. Soft Matter 2011;7(11):5246–54.

[2] Zubarev AY. Effect of chain-like aggregates on ferrogel magnetodeformation. Soft Matter 2013;9(20):4985–92.

[3] Pang H, Pei L, Sun C, Gong X. Normal stress in magnetorheological polymer gel under large amplitude oscillatory shear. J. Rheol. 2018;62(6):1409–18.

[4] Ding Li, Pei L, Xuan S, Fan X, Cao X, Wang Yu, et al. Ultrasensitive Multifunctional Magnetoresistive Strain Sensor Based on Hair-Like Magnetization-Induced Pillar Forests. Adv. Electron Mater 2020;6(1):1900653. https://doi.org/10.1002/aelm.v6.110.1002/aelm.201900653.

[5] Jang D, Farooq SZ, Yoon HN, Khalid HR. Design of a highly flexible and sensitive multi-functional polymeric sensor incorporating CNTs and carbonyl iron powder. Compos. Sci. Technol. 2021;207:108725. https://doi.org/10.1016/j.compscitech.2021.108725.

[6] Hu T, Xuan S, Shu Q, Xu Z, Shen L, Li J, et al. Triple-shape memory, magneto-response, and piezo-resistive flexible composites: multiple-sensing and switchable actuating. J. Mater. Chem. C 2021;9(20):6568–78.

[7] Qi S, Fu J, Xie Y, Li Y, Gan R, Yu M. Versatile magnetorheological plastomer with 3D printability, switchable mechanics, shape memory, and self-healing capacity. Compos. Sci. Technol. 2019;183:107817. https://doi.org/10.1016/j.compscitech.2019.107817.

[8] Wang L, Zheng DC, Harker P, Patel AB, Guo CF, Zhao XH. Evolutionary design of magnetic soft continuum robots. Proc Nat Acad Sci USA 2021;118(21):e2021922118.

[9] Kim Y, Yuk H, Zhao R, Chester SA, Zhao X. Printing ferromagnetic domains for untethered fast-transforming soft materials. Nat. 2018;558(7709):274–9.

[10] Xu J, Xuan S, Pang H, Gong X. The strengthening effect of 1D carbon materials on magnetorheological plastomers: mechanical properties and conductivity. Smart Mater Struct. 2017;26(3):035044. https://doi.org/10.1088/1361-665X/aa5bd6.

[11] Pang H, Xuan S, Liu T, Gong X. Magnetic field dependent electro-conductivity of the graphite doped magnetorheological plastomers. Soft Matter 2015;11(34):6893–902.

[12] Xu J, Pang H, Gong X, Pei L, Xuan S. A shape-deformable liquid-metal-filled magnetorheological plastomer sensor with a magnetic field "on-off" switch. iSci. 2021;24(6):102549. https://doi.org/10.1016/j.isci.2021.102549.

[13] Yu M, Yang P, Fu J, Liu S. Flower-like carbonyl iron powder modified by nanoflakes: Preparation and microwave absorption properties. Appl. Phys. Lett. 2015;106(16):161904. https://doi.org/10.1063/1.4919064.

[14] Wang L-R, Yu M, Yang P-A, Qi S, Fu J. Synthesis of absorbing coating based on magnetorheological gel with controllable electromagnetic wave absorption properties. Smart Mater Struct. 2019;28(4):044001. https://doi.org/10.1088/1361-665X/ab06e8.

[15] Zhang X, Qi S, Zhao Yi, Wang L, Fu J, Yu M. Synthesis and microwave absorption properties of Fe@carbon fibers. RSC Adv. 2020;10(54):32561–8.

[16] Sun C, Pang H, Xuan S, Gong X. Glass microspheres strengthened magnetorheological plastomers for sound insulation. Mater Lett. 2019;256:126611. https://doi.org/10.1016/j.matlet.2019.126611.

[17] Xie Y, Yu M, Qu H, Fu J. Carbon black reinforced magnetorheological gel enabled high-performance magneto-resistor for motor soft start-up. Smart Mater Struct. 2019;28(12):125019. https://doi.org/10.1088/1361-665X/ab4231.

[18] Zhang Lu, Liu W, Wen X, Chen J, Zhao C, Castillo-Rodríguez M, et al. Electrospun submicron NiO fibers combined with nanosized carbon black as reinforcement for multi-functional poly(lactic acid) composites. Compos. Part A Appl. S 2020;129:105662. https://doi.org/10.1016/j.compositesa:2019.105662.

[19] Chen Y-F, Li J, Tan Y-J, Cai J-H, Tang X-H, Liu J-H, et al. Achieving highly electrical conductivity and piezoresistive sensitivity in polydimethylsiloxane/multi-walled carbon nanotube composites via the incorporation of silicon dioxide micro-particles. Compos. Sci. Technol. 2019;177:41–8.

[20] Rankin SM, Moody MK, Naskar AK, Bowland CC. Enhancing functionalities in carbon fiber composites by titanium dioxide nanoparticles. Compos. Sci. Technol. 2021;201:108491. https://doi.org/10.1016/j.compscitech.2020.108491.

[21] Chortos A, Mao J, Mueller J, Hajiesmaili E, Lewis JA, Clarke DR. Printing Reconfigurable Bundles of Dielectric Elastomer Fibers. Adv. Funct. Mater 2021;31(22):2010643. https://doi.org/10.1002/adfm.v31.2210.1002/adfm.202010643.

[22] Pang H, Xu Z, Shen L, Li J, Zhang J, Li Z, et al. The dynamic compressive properties of magnetorheological plastomers: enhanced magnetic-induced stresses by non-magnetic particles. J. Mater Sci. Technol. 2022;102:195–203.

[23] Ulicny JC, Snavely KS, Golden MA, Klingenberg DJ. Enhancing magnetorheology with nonmagnetizable particles. Appl. Phys. Lett. 2010;96(23):231903. https://doi.org/10.1063/1.3431608.

[24] Mitsumata T, Ohori S, Chiba N, Kawai M. Enhancement of magnetoelastic behavior of bimodal magnetic elastomers by stress transfer via nonmagnetic particles. Soft Matter 2013;9(42):10108–16.

[25] Nagashima K, Kanauchi S, Kawai M, Mitsumata T, Tamesue S, Yamauchi T. Nonmagnetic particles enhance magnetoelastic response of magnetic elastomers. J. Appl. Phys. 2015;118(2):024903. https://doi.org/10.1063/1.4926646.

[26] Rodríguez-Arco L, López-López MT, Zubarev AY, Gdula K, Durán JDG. Inverse magnetorheological fluids. Soft Matter 2014;10(33):6256–65.

[27] Keaveny EE, Maxey MR. Modeling the magnetic interactions between paramagnetic beads in magnetorheological fluids. J. Comput. Phys. 2008;227(22):9554–71.

[28] Tan C, Jones TB. Interparticle Force Measurements on Ferromagnetic Steel Balls. J. Appl. Phys. 1993;73(8):3593–8.

[29] Ginder JM, Davis LC. Shear Stresses in Magnetorheological Fluids - Role of Magnetic Saturation. Appl. Phys. Lett. 1994;65(26):3410–2.

[30] Peng X, Min Y, Ma T, Luo W, Yan Mi. Two-dimensional Monte Carlo simulations of structures of a suspension comprised of magnetic and nonmagnetic particles in uniform magnetic fields. J. Magn. Magn. Mater 2009;321(9):1221–6.

[31] Liu T, Gong X, Xu Y, Xuan S. Magneto-induced stress enhancing effect in a colloidal suspension of paramagnetic and superparamagnetic particles dispersed in a ferrofluid medium. Soft Matter 2014;10(6):813–8.

[32] Shixu Li, Jing Z, Jun L, Jie Fu, Miao Yu, Song Qi. Enhancing Effect of Fe3O4/Nanolignocelluloses in Magnetorheological Fluid. Langmuir 2021;37(23):7176–84.

[33] Liu TX, Gong XL, Xu YG, Xuan SH, Jiang WQ. Simulation of magneto-induced rearrangeable microstructures of magnetorheological plastomers. Soft Matter 2013;9(42):10069–80.

[34] Klingenberg DJ, Olk CH, Golden MA, Ulicny JC. Effects of nonmagnetic interparticle forces on magnetorheologicalfluids. J. Phys. Condens Matter 2010;22(32):324101. https://doi.org/10.1088/0953-8984/22/32/324101.

[35] Mori T, Tanaka K. Average Stress in Matrix and Average Elastic Energy of Materials with Misfitting Inclusions. Acta. Metall. 1973;21(5):571–4.